# Intermetallics of 4:4:1 and 3:3:1 series in La–(Co,Ni)–M (M = Bi, Pb, Te, Sb, Sn and Ga, Al) systems and their properties

Vitalii Shtender, Volodymyr Smetana, Jean-Claude Crivello, Anatolii Kravets, Łukasz Gondek, Anja-Verena Mudring, Martin Sahlberg

**Intermetallics of 4:4:1 and 3:3:1 series in La–(Co,Ni)–*M* (*M* = Bi, Pb, Te, Sb, Sn and Ga, Al) systems and their properties**

Vitalii Shtender[1,*], Volodymyr Smetana[2,3,*], Jean-Claude Crivello[4,5], Anatolii Kravets[6,7], Łukasz Gondek[8], Anja-Verena Mudring[2,3], Martin Sahlberg[1]

[1]*Department of Chemistry – Ångström Laboratory, Uppsala University, Box 538, 751 21, Uppsala, Sweden*

[2]*Department of Materials and Environmental Chemistry, Stockholm University, Svante Arrhenius väg 16c, 10691 Stockholm, Sweden*

[3]*Department of Biological and Chemical Engineering and iNANO, Aarhus University, 8000, Aarhus C, Denmark*

[4]*Univ Paris Est Creteil, CNRS, ICMPE, UMR7182, 2 rue Henri Dunant, 94320 Thiais, France*

[5]*CNRS-Saint-Gobain-NIMS, IRL 3629, Laboratory for Innovative Key Materials and Structures (LINK), 1-1 Namiki, 305-0044 Tsukuba, Japan*

[6]*Nanostructure Physics, Royal Institute of Technology, 10691, Stockholm, Sweden*

[7]*Institute of Magnetism of the NAS of Ukraine and MES of Ukraine, 03142 Kyiv, Ukraine*

[8]*AGH University of Krakow, Faculty of Physics and Applied Computer Science, Mickiewicza 30, 30-059, Krakow, Poland*

Dedicated to the memory of Prof. **Vitalij K. Pecharsky**

*Corresponding author: vitalii.shtender@angstrom.uu.se, vs@bce.au.dk

# Abstract

Two series of isostructural intermetallics have been discovered in our search for new compounds with fused honeycomb motifs, both stable at elevated temperatures (1073 K). Both crystallize with orthorhombic unit cells – $La_4Co_4M$ (*M* = Sn, Sb, Te, Pb, Bi, SG *Pbam*, *a* = 8.247–8.315(2), *b* = 21.913–22.137(7), *c* = 4.750–4.664(2) Å, *V* = 850.5–869.5(4) Å$^3$, *Z* = 4) and $La_3Ni_3M$ (*M* = Al, Ga, SG *Cmcm*, *a* = 4.1790–4.2395(1), *b* = 10.4921–10.6426(6), *c* = 13.6399–13.7616(8) Å, *V* = 606.72–612.05(7), *Z* = 3). The crystal structures represent interesting variations of semiregular tilings of corrugated anionic layers and predominantly cationic zigzag motifs. The $La_4Co_4M$ compounds reveal a complex type of ordering with a high degree of frustration as could be expected for the Kagomé-related lattices, while magnetic ordering in the $La_3Ni_3M$ series is less evident. Electronic structure calculations have been performed for multiple compounds within both series revealing metallic character and visible local minima around the Fermi level. The bonding picture is characterized by nearly equal contributions from the anionic and the cationic components.

***Keywords***: *Intermetallics, crystal structure, electronic structure, magnetic properties.*

# 1. Introduction

Polar intermetallic compounds have been extensively investigated exhibiting broad compositional variability and enormous structural complexity [1]. While usually polar intermetallics include a wide range of compounds extending from the metal alloys to Zintl compounds [2], considerable attention has been paid to the middle range, compounds with the valence electron count of around 2 [3, 4]. This group is mostly represented by ternary compounds including active or rare-earth metals, transition metals and a *p*-block element including some metalloids [5-8]. Among them, trielides and tetrelides are the most frequent and offer a plethora of structural motifs of all dimensionalities, *i.e.* from clusters to networks and peculiar bonding features [1]. Besides compositional wealth such element combination is also interesting in terms of properties. Superconductivity has been detected for many *p* elements and their compounds, *e.g.* the majority of the La-Sn binary compounds [9-11]. On the other hand, rare earth elements, with their high number of unpaired *f*-electrons, are most important for introducing magnetism. Adding transition metals allows, aside from magnetism, to add additional features including electronic and geometric adjustments leading to interesting properties and unique property combinations. For example, though containing a magnetic element Co, LaCoSi exhibits superconductivity 4 K [12]. It is also known as a catalyst for $NH_3$ production [13].

Until now, none of La–(Co,Ni)–*M* (*M* = Bi, Pb, Te, Sb, Sn and Ga, Al) ternary systems have been fully explored [14]. So far, systems with Bi and Te have only one representative each: $La_6Co_{13}Bi$ [15] and $La_6CoTe_2$ [16]. Systems with Pb and Sb are presented with three and four compounds, respectively: $La_6Co_{13}Pb$ [15], $La_5CoPb_3$ [17], $La_{12}Co_6Pb$ [18], and $La_6Co_{13}Sb$ [15], $LaCo_xSb_2$ [19], $LaCoSb_3$ [20], $La_xCo_4Sb_{12-y}$ [21]. For the Sn-based system, six compounds were already reported: $La_6Co_{13}Sn$ [15], $La_4Co_2Sn_5$ [22], $La_{117}Co_{67}Sn_{113}$ [23], $LaCo_xSn_2$, $La_3Co_2Sn_7$ [24] and $La_3Co_4Sn_{13}$ [25]. In contrast, the La-Co-*M* (*M* = Bi, Pb, Te, Sb and Sn) systems, and the La-Ni-*M* (*M* = Ga and Al) systems were studied to a wider extent. For instance, the Ga-based systems presented by: $La_3Ni_2Ga_2$, $La_3Ni_4Ga_2$ [26], $La_2Ni_{2.25}Ga_{0.75}$ [27], $LaNi_4Ga$ [28], LaNiGa, $LaNi_{11}Ga_2$ [29], $LaNi_3Ga_2$, $LaNiGa_2$ [30], $LaNi_{2.4}Ga_{2.6}$ [31], $LaNi_{2-x}Ga_{2+x}$, $LaNi_9Ga_4$ and $LaNi_{5.5}Ga_{7.5}$ [29], $LaNi_{7.25}Ga_{5.75}$ [29], $La_2NiGa_{12}$ [32], $La_2NiGa_{10}$ [33] and $La_2Ni_{13}Ga_{13}$ [29]. Finally, the system with Al so far is presented with: $LaNi_{5-x}Al_x$ [34], $La_2Ni_{2.25}Al_{0.75}$ [27], $La_5Ni_2Al_3$ [35], $La_3Ni_4Al_2$ [36], LaNiAl [37], $LaNiAl_2$ [38], $LaNi_2Al_3$ [39], $LaNi_2Al_5$ [40], $LaNi_{1.44}Al_{5.56}$ [41], and $La_2NiAl_7$ [42].

Despite the number of discovered compounds, their physical or chemical properties have been investigated to an even lesser extent. The most interesting are ferromagnetism in $La_6Co_{13}M$ [15] and $La_4Co_2Sn_5$ [22], low thermal conductivity in the La-filled cobalt antimonide Skutterudites $La_xCo_4Sb_{12}$ [43], superconductivity in $La_3Co_4Sn_{13}$, and largely positive and

nonsaturating magnetoresistance of $La_2NiGa_{12}$ [32]. Some other compounds, e.g. $LaNi_4Ga$ [44] or $LaNi_4Al$ [45] showed good hydrogen sorption efficiency. In the latter case, hydrogenation influenced the magnetic properties leading to ferromagnetism [46]. $LaNi_3Ga_2$ reveals spin fluctuation [47] while excellent MCE (magnetocaloric effect) performance has been observed in a series of $R_2T_2X$ [48]. Magnetic properties have also been inspected in $LaNi_{0.75}Ga_{3.25}$ [49], $LaNiAl_2$ [50], $R_2Ni_2Ga$ and $R_2Ni_2Al$ [27].

In the present work, we explored two series of isotypic ternary compounds in the La–(Co,Ni)–*M* systems *i.e.* $La_4Co_4M$ and $La_3Ni_3M$ (*M* = Bi, Pb, Te, Sb, Sn and Ga, Al). Although isocompositional compounds are quite common in these systems, it is interesting to note that the discovery of the $La_4Co_4M$ series brought us to the fact that such types of compounds can be obtained with 'antagonistic pairs' [51] (like Co-Pb or Co-Bi). Following the structural studies, magnetic behavior as well as electronic structures have been investigated for both series.

## 2. Experimental part and theoretical methods

The $La_4Co_4Sn$ and $La_3Ni_3M$ (*M*= Ga and Al) alloys (1g each) were synthesized by arc-melting of high purity La (99.9%), Ni and Co (99.99%), Sn, Ga and Al (99.999%) with further annealing at 800 °C in vacuum. The observed weight losses never exceeded 0.5 %. The $La_4Co_4M$ (*M*= Bi, Pb, Te and Sb) alloys were prepared from arc-melted $La_4Co_4$ ligature and Bi, Pb, Te and Sb (all with 99.9% purity) powders to avoid evaporation losses during heating. The ligatures were crushed and mixed with the respective *M*-metals. Such mixtures were loaded into Ta tubes and sealed under Ar atmosphere. Ta tubes were afterward placed in stainless steel tubes to protect them from oxidation. The samples were heated up to 1073 K for 10h, kept for 10h at 1073 K and cooled to 773 K at 3 K/h. Final cooling has been performed by switching off the furnace.

Intensity data sets for powder X-ray diffraction (PXRD) were recorded at room temperature using a Bruker D8 X-ray diffractometer with a Lynx-eye position sensitive detector and Cu-Kα radiation on a zero-background single crystal Si sample holder. Phase analyses using the Rietveld method [52] of the powder X-ray data were performed using Topas 6 software [53]. Rietveld refinements of selected samples are presented in Supporting Information (SI) **Figure S1**.

Single-crystal X-ray diffraction (SCXRD) data were collected at 293 K on a Bruker D8 Venture diffractometer (Bruker, USA; Photon 100 CMOS detector, IμS microfocus source: Mo $K_\alpha$ radiation, $\lambda$ = 0.71073 Å, 2 –5). Intensity data sets of reflections and scaling were integrated within the APEX3 software package by using SAINT [54]. Absorption corrections were conducted with SADABS [55] and crystal structure solutions with SHELXT [56]. For subsequent difference, Fourier analyses and least-squares refinements, SHELXL-2013 [57] was

used. The experimental details of the crystal structure determination and refinement as well as the atomic coordinates for $La_4Co_4Bi$ and $La_3Ni_3Ga$ as representative examples have been collected in **Tables 1** and **2**.

The microstructure was evaluated with a Zeiss Merlin SEM equipped with a secondary electron (SE) detector and an energy-dispersive X-ray (EDX) spectrometer. The samples for electron microscopy analysis were prepared by standard metallographic techniques through grinding with SiC paper. For the final polishing, a mixture of $SiO_2$ and $H_2O$ was used. SEM micrographs are presented in **Figure S2**.

Magnetization measurements were conducted using a Physical Property Measurement System (PPMS, Quantum Design, USA). Vibrating Sample Magnetometer (VSM) options were utilized to measure zero-field cooled (ZFC) and field-cooled (FC) magnetization between 2 and 300 K in static fields (DC) up to 7 T. Isothermal magnetization was acquired in applied fields up to 7 T. Polycrystalline samples were filled into polypropylene (PP) capsules, which were mounted into a brass sample holder.

The First-Principles calculations have been led in a similar way to the previous work [58], using the VASP code [59, 60], *i.e.* the electronic properties were determined through Density Functional Theory (DFT) using a pseudopotential approach within the projector augmented-wave (PAW) method, employing collinear spin polarization. The Perdew-Burke-Ernzerhof (PBE) functional [61] in the generalized gradient approximation (GGA), was employed with a cutoff energy of 600 eV. Structural relaxations, encompassing volume, cell shape, and atomic positions, were performed while maintaining the original symmetry, with a convergence criterion set at forces less than 0.05 meV per Å. Crystal orbital Hamiltonian population (COHP) curves were extracted by the Lobster program [62]. Subsequently, phonon calculations were conducted within the harmonic approximation for $La_3Ni_3Ga$ and $La_4Co_4Bi$ using a supercell approach (2×2×1, 1×1×2 respectively), as implemented with the Phonopy code [63]. Charge transfer analyses were carried out following Bader's method [64].

**Table 1**. Crystallographic data and experimental details of the structure determination for the $La_4Co_4M$ and $La_3Ni_3M$ ($M$ = Bi, Pb, Te, Sb, Sn and Ga, Al). Experiments were carried out at 293 K with Mo $K\alpha$ radiation.

| Empirical formula | **$La_4Co_4Bi$** | **$La_4Co_4Pb$** | **$La_4Co_4Te$** | **$La_4Co_4Sb$** | **$La_4Co_4Sn$** | **$La_3Ni_3Al$** | **$La_3Ni_3Ga$** |
|---|---|---|---|---|---|---|---|
| CSD | 2301799 | 2301803 | 2301805 | 2301804 | 2301802 | 2301800 | 2301801 |
| Composition at.% from EDX | $La_{45.3(3)}Co_{43.4(3)}Bi_{11.3(1)}$ | $La_{45.3(3)}Co_{42.7(6)}Pb_{12.0(6)}$ | $La_{45.4(5)}Co_{43.4(3)}Te_{11.3(3)}$ | $La_{45.1(2)}Co_{43.6(4)}Sb_{11.3(3)}$ | $La_{45.0(2)}Co_{43.8(2)}Sn_{11.3(2)}$ | $La_{44.0(4)}Ni_{41.7(6)}Al_{14.3(3)}$ | $La_{42.8(5)}Ni_{42.8(4)}Ga_{14.4(5)}$ |
| Structure type | Own | $La_4Co_4Bi$ | $La_4Co_4Bi$ | $La_4Co_4Bi$ | $La_4Co_4Bi$ | $Er_3Ge_4$ | $Er_3Ge_4$ |
| Formula weight, Mr (g/mol) | 1000.34 | 998.55 | 918.96 | 913.11 | 910.05 | 619.84 | 662.58 |
| Space group (No.) | *Pbam* (55) | *Pbam* (55) | *Pbam* (55) | *Pbam* (55) | *Pbam* (55) | *Cmcm* (63) | *Cmcm* (63) |
| Pearson symbol, $Z$ | *oP*36, 4 | *oP*36, 4 | *oP*36, 4 | *oP*36, 4 | *oP*36, 4 | *oS*28, 4 | *oS*28, 4 |
| $a$, Å | 8.315(1) | 8.269(3) | 8.274(3) | 8.249(2) | 8.247(2) | 4.1790(1) | 4.2395(3) |
| $b$, Å | 22.137(4) | 21.961(7) | 22.0394(4) | 21.930(3) | 21.913(7) | 10.6426(3) | 10.4921(6) |
| $c$, Å | 4.724(1) | 4.749(2) | 4.6638(8) | 4.7060(8) | 4.745(1) | 13.7616(4) | 13.6399(8) |
| $V$, Å$^3$ | 869.5(3) | 862.5(5) | 850.5(4) | 851.3(3) | 857.5(4) | 612.05(3) | 606.72(7) |
| Calculated density, $\rho$ (g·cm$^{-3}$) | 7.64 | 7.69 | 7.18 | 7.12 | 7.05 | 6.73 | 7.25 |
| Absorption coefficient, $\mu$ (mm$^{-1}$) | 46.67 | 46.17 | 30.48 | 30.19 | 29.74 | 29.50 | 33.96 |
| Theta range (°) | 2.617 ÷ 27.494 | 2.632 ÷ 30.000 | 1.848 ÷ 32.679 | 2.638 ÷ 30.505 | 2.639 ÷ 30.664 | 2.960 ÷ 29.978 | 2.987 ÷ 29.975 |
| $F$(000) | 1676 | 1672 | 1552 | 1548 | 1544 | 1072 | 1144 |
| Range in $h$ $k$ $l$ | $-10 \le h \le 8$,<br>$-28 \le k \le 23$,<br>$-4 \le l \le 6$ | $-11 \le h \le 11$,<br>$-26 \le k \le 29$,<br>$-6 \le l \le 6$ | $-12 \le h \le 12$,<br>$-33 \le k \le 33$,<br>$-6 \le l \le 7$ | $-9 \le h \le 11$,<br>$-24 \le k \le 31$,<br>$-6 \le l \le 6$ | $-11 \le h \le 10$,<br>$-31 \le k \le 31$,<br>$-6 \le l \le 5$ | $-5 \le h \le 5$,<br>$-14 \le k \le 14$,<br>$-19 \le l \le 19$ | $-5 \le h \le 5$,<br>$-14 \le k \le 14$,<br>$-18 \le l \le 19$ |
| Total No. of reflections | 6252 | 10397 | 12773 | 9467 | 10437 | 4265 | 4195 |
| No. of independent reflections | 1115 ($R_{eq}$ = 0.0640) | 1387 ($R_{eq}$ = 0.0823) | 1717 ($R_{eq}$ = 0.0147) | 1439 ($R_{eq}$ = 0.0747) | 1470 ($R_{eq}$ = 0.0584) | 517 ($R_{eq}$ = 0.0276) | 508 ($R_{eq}$ = 0.0483) |
| No. of reflections with $I > 2\sigma(I)$ | 918 ($R_{\sigma}$ = 0.0495) | 1104 ($R_{\sigma}$ = 0.0548) | 1684 ($R_{\sigma}$ = 0.0088) | 1175 ($R_{\sigma}$ = 0.0523) | 1224 ($R_{\sigma}$ = 0.0407) | 516 ($R_{\sigma}$ = 0.0208) | 507 ($R_{sigma}$ = 0.0282) |
| Data/parameters | 1115/55 | 1387/55 | 1717/55 | 1439/55 | 1470/55 | 517/26 | 508/26 |
| Goodness-of-fit on $F^2$ | 1.054 | 1.103 | 1.080 | 1.052 | 1.088 | 1.273 | 1.344 |
| Final $R$ indices [$I > 2\sigma(I)$] | $R_1$ = 0.0311;<br>w$R_2$ = 0.0375 | $R_1$ = 0.0364;<br>w$R_2$ = 0.0446 | $R_1$ = 0.0110;<br>w$R_2$ = 0.0215 | $R_1$ = 0.0349;<br>w$R_2$ = 0.0548 | $R_1$ = 0.0291;<br>w$R_2$ = 0.0368 | $R_1$ = 0.0145;<br>w$R_2$ = 0.0443 | $R_1$ = 0.0206;<br>w$R_2$ = 0.0481 |
| $R$ indices (all data) | $R_1$ = 0.0464;<br>w$R_2$ = 0.0394 | $R_1$ = 0.0597;<br>w$R_2$ = 0.0471 | $R_1$ = 0.0116;<br>w$R_2$ = 0.0219 | $R_1$ = 0.0526;<br>w$R_2$ = 0.0586 | $R_1$ = 0.0447;<br>w$R_2$ = 0.0390 | $R_1$ = 0.0145;<br>w$R_2$ = 0.0443 | $R_1$ = 0.0208;<br>w$R_2$ = 0.0482 |
| Extinction coefficient | 0.00134(4) | 0.00059(3) | 0.00032(2) | 0.00171(9) | 0.00086(4) | 0.0012(1) | 0.0010(2) |

**Table 2**. Atomic coordinates and equivalent isotropic displacement parameters for the $La_4Co_4Bi$ and $La_3Ni_3Ga$ compounds as representative models for the corresponding isostructural series.

| Atom | Site | *x* | *y* | *z* | $U_{eq}$ (Å$^2$) |
|---|---|---|---|---|---|
| | | | **$La_4Co_4Bi$** | | |
| La1 | 4*h* | 0.27768(8) | 0.15043(3) | ½ | 0.0101(2) |
| La2 | 4*h* | 0.40848(8) | 0.42431(3) | ½ | 0.0082(2) |
| La3 | 4*g* | 0.06761(8) | 0.42052(3) | 0 | 0.0106(2) |
| La4 | 4*g* | 0.44744(8) | 0.27701(3) | 0 | 0.0079(2) |
| Co1 | 8*i* | 0.25659(13) | 0.02919(5) | 0.2492(2) | 0.0086(2) |
| Co2 | 4*g* | 0.1037(2) | 0.10918(7) | 0 | 0.0129(4) |
| Co3 | 2*d* | 0 | ½ | ½ | 0.0089(5) |
| Co4 | 2*a* | 0 | 0 | 0 | 0.0099(5) |
| Bi | 4*h* | 0.16016(5) | 0.30108(2) | ½ | 0.0080(1) |
| | | | **$La_3Ni_3Ga$** | | |
| La1 | 8*f* | 0 | 0.28250(3) | 0.60309(2) | 0.01215(6) |
| La2 | 4*c* | 0 | 0.00101(5) | ¼ | 0.01310(7) |
| Ni1 | 8*f* | 0 | 0.43151(8) | 0.08559(6) | 0.01262(9) |
| Ni2 | 4*c* | 0 | 0.30527(9) | ¼ | 0.0140(1) |
| Ga | 4*a* | 0 | 0 | 0 | 0.0098(1) |

# 3. Results and discussion

*3.1 Crystal structures*

As to the extent of our knowledge, the intriguing hexagonal honeycomb-like structure motifs extending along the 6(3)-fold axis were first observed in $La_{15}Ni_{13}Bi_5$ [58], we extended our explorations onto chemically closely related systems. Although identical motifs could not be observed in any of them, two isostructural series were identified, *i.e.* $La_4Co_4M$ (*M* = Bi, Pb, Te, Sb and Sn) and $La_3Ni_3M$ (*M* = Ga and Al). Both of them crystallize with orthorhombic unit cells though different space groups, *Pbam* and *Cmcm*, respectively (**Table 1**). While $La_3Ni_3M$ are ordered ternary representatives of the $Er_3Ge_4$ type [65], $La_4Co_4M$ are the first representatives of their own type of structure.

The crystal structure of $La_4Co_4Bi$ (as a representative of the $La_4Co_4M$ series) is best described in terms of relatively separated Co and Bi layers well in line with the antagonistic nature [51] of this pair stacking along the *b* axis (**Figure 1**). Bi atoms form zigzag chains along the *a* axis being surrounded by La equatorially tricapped prisms. Such a zigzag sequence of the prisms also leaves tetrahedral voids appearing like a distorted $(3.6)^2$ Kagomé-like ribbon. It is worth noting that such a *p*-element-centered trigonal prism is a common structural element in an extended family of intermetallics, though they usually condense forming larger triangular conglomerates with an edge size of up to six units [66, 67]. It is interesting that unit cell of $La_4Co_4M$ contracts from Sn to Sb and Te, however, the unit cell shape change is strongly

anisotropic where the *a* parameter is the least affected, the *b* expands and the *c* contracts (**Table 1**).

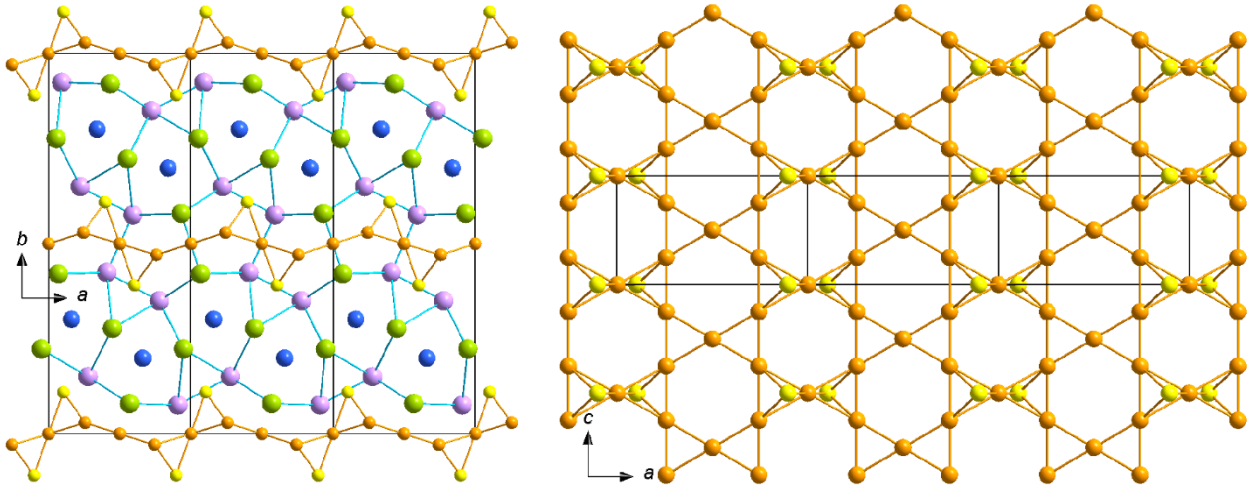


**Figure 1**. Projection of the crystal structure of $La_4Co_4Bi$ on the *ab* plane (left) and Co Kagomé lattice (right). La atoms are green and lavender, Co – orange and yellow, and Bi – blue.

The cobalt layer represents a slightly corrugated augmented Kagomé lattice (**Figure 1 (right)**) separating the triangular La/Bi motifs. Due to additional capping Co atoms (yellow), Co hexagons and triangles show a little different degree of distortion with Co-Co distances 2.3544–2.4326(8) Å and 2.3544–2.5211(8) Å, respectively. It is worth noting that none of these distances exceed the sum of two covalent radii of Co (1.27 Å) [68]. The Co-Co-Co angles within the hexagons do not deviate significantly from the ideal 120° angle – 119.3–121.7(1) and 117.8–124.3(1)°, however, the angles between the neighboring hexagons along the *a* axis are 143.4(1)°, quite noticeably deviating from planarity.

The crystal structure of $La_3Ni_3Ga$ exhibits analogous puckered but polyanionic layers separated by the layers of edge-sharing square pyramids. The latter extend along the *a* axis but alternate their orientation along the *c* (**Figure 2**). More interesting are the polyanionic motifs exhibiting a mix of a planar arrangement of $Y_2Co_2Ga$ [69] and zigzag corrugation of $La_4Co_4Bi$. Although the $Er_3Ge_4$ structure type is not rare with the smaller rare earth metals, *e.g.* Y [70], our compound is just the second representative of this type with La following $La_3Ni_3Zn$ [71]. The tiling of the anionic layers is now $3^28^2$; however, the 8-membered corrugated $Ni_6Ga_2$ octagon is in fact a truncated version of two fused hexagons (Figure S3) with the mechanism observed in $La_{15}Ni_{13}Bi_5$ [58]. The truncated vertices are analogously compensated with the La atoms. All angles within the octagons show a slightly more significant deviation from 120° but only due to the presence of the second type atoms in the network (112.8–123.5(1)°) where the angles between the hexagons are even more regular – 118.5(1)°. It is though interesting that Ni-Ni distances are relatively long (>2.6 Å) exceeding the sum of the covalent radii (1.26 Å) indicating significant influence of the heteroatomic anionic component.

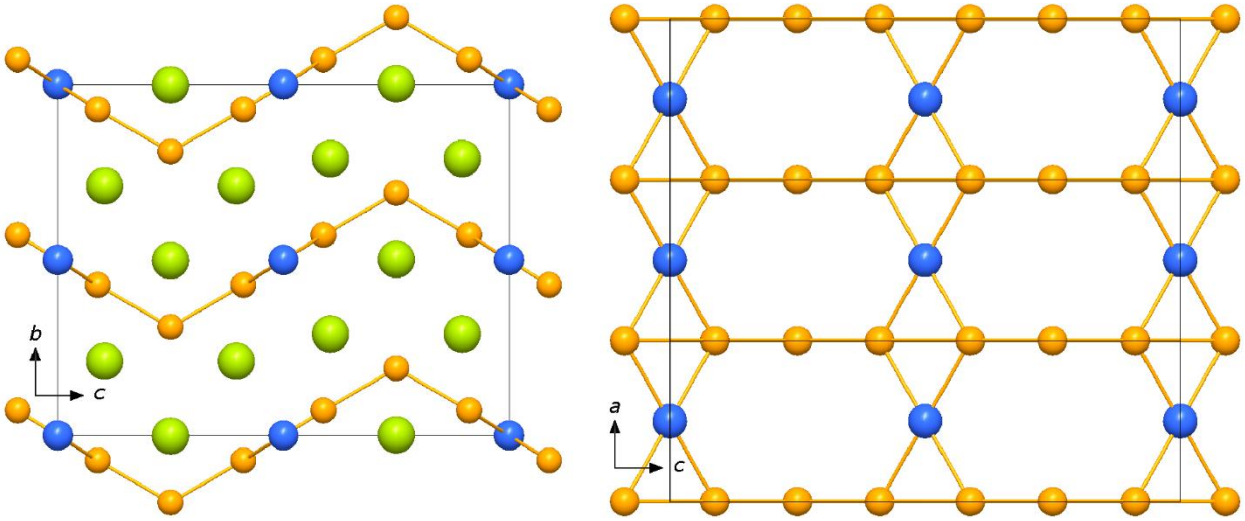


**Figure 2**. Projection of the crystal structure of $La_3Ni_3Ga$ on the *bc* plane (left) and Co/Ga $3^2 8^2$ lattice (right). La atoms are green and lavender, Ni – orange and Ga – blue.

Kagomé lattice compounds, particularly but not limited to intermetallics ones, attracted a lot of attention in recent years due to the fascinating physics they can reveal [72-77]. Although the $La_4Co_4Bi$ type is new, an identical corrugated kagomé lattice has been observed in the binary $La_2Co_3$ [78]. From the common features, we must outline that the homoatomic Co network corrugation in both structures is interconnected with the cationic zigzag motifs. $La_2Co_3$ exhibits similar hexagonal motifs though in the form of homogeneous slightly distorted honeycombs along the *a* axis. Contrary, the lattice in $Y_2Co_2Ga$ [69] is planar but composed of two elements and shows a bit different tiling scheme – $3^2 6^2$ (**Figure 3**). Apparently, such a tiling scheme is more resistant and can accommodate corrugated cationic motifs keeping the network planarity. More complex augmented or even sandwiched kagomé lattices have been observed in the series of intermetallics Eu$T_5$In ($T$ = Cu, Ni) [79, 80] also revealing complex magnetic structures.

Related corrugated tilings with truncated hexagonal fragments may extend to $3^2 10^2$ or even $3^2 12^2$ (**Figure 3**) as observed in the crystal structures of $Y_4Co_4Ga$ and $Y_5Co_5Ga$ or their derivatives, respectively [81, 82]. Their corrugations involve multiple truncated hexagons including those with two missing vertices in $Y_5Co_5Ga$ with even more differentiated shapes. Each missing vertex is again compensated by a rare-earth atom from the interlayer space. In this series, the planar tiling in $Y_2Co_2Ga$ shows the highest degree of distortion and extremely short Co-Co distances suggesting possible underoccupation of some positions. Following the general tendency, all Co-Co-Co angles in the corrugated layers show a minimal degree of distortion not exceeding 3° from the ideal hexagonal angle. Contrary, the heteroatomic component always leads to a more significant distortion and some stretching of the ribbon ($\angle_{Co\text{-}Ga\text{-}Co}$ = 112.5–115.5°).

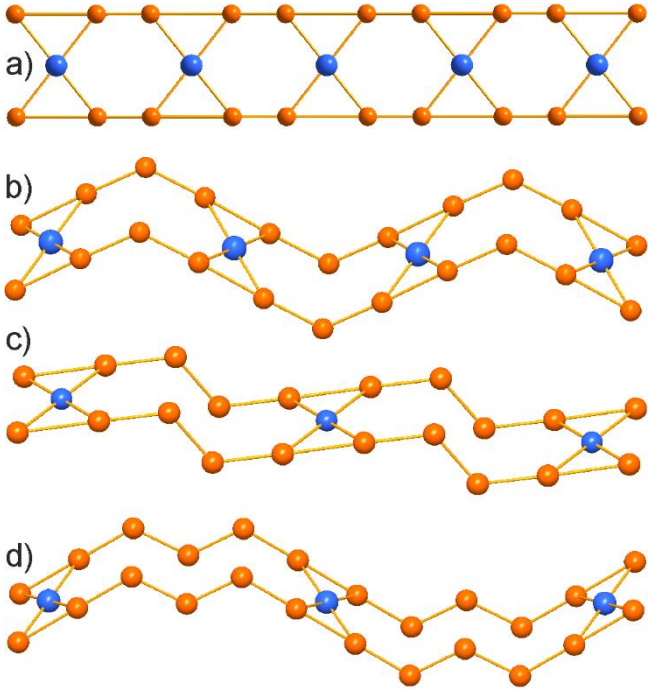


**Figure 3.** $3^2 6^2$, $3^2 8^2$, $3^2 10^2$ and $3^2 12^2$ type ribbons stacking into layers in the crystal structures of $Y_2Co_2Ga$ (a), $La_3Ni_3Ga/Y_3Co_3Ga$ (b), $Y_4Co_4Ga$ (c) and $Y_5Co_5Ga$ (d), respectively. Transition metals are colored orange and Ga – blue.

*3.2 Magnetic properties*

Magnetic properties of the investigated $La_4Co_4M$ with $M$ = Sb, Pb and Bi are presented in **Figure 4**. For low measuring fields the properties of $La_4Co_4Sb$ were biased by small impurity of $La_2Co_{1.7}$ [83] (**Table S1**). Therefore, on the **Figure 4a** susceptibility measured at 5 T is presented. It shows a distinct anomaly at 170 K suggesting occurrence of antiferromagnetic ordering below that temperature. At lowest temperatures the susceptibility shows a small increase, which presumably is connected to some reorientation of magnetic moments. Inverse susceptibility follows the Curie-Weiss (CW) law down to 220 K, with the paramagnetic Curie temperature ($\theta_{CW}$) as low as -79.8(1) K, the effective magnetic moment was found to be 7.0(0) $\mu_B$ per f.u. Assuming that only Co atoms are magnetic, it means that mean value per Co atoms is about 1.75 $\mu_B$, which is close to typical values for low-spin $Co^{2+}$ configuration. Isothermal magnetization measured at 2 K shows soft magnetic contribution overlaid on the antiferromagnetic (AF)-like, non-saturating behavior. The soft magnetic properties are likely related to aforementioned rise of magnetic susceptibility at low temperatures. In general, soft magnetic properties are not very surprising as strong AF interaction is usually restricted to Kagomé lattices, whereas inter-planar coupling can be way weaker, yet even ferromagnetic.

To some extent, the situation evidenced for $La_4Co_4Pb$ is similar (**Figure 4b**). The departure of ZFC and FC (field cooled) curves observed at 170 K is likely connected to the occurrence of a minority ferromagnetic phase $La_6Co_{13}Pb$ [15], while the real ordering temperature seems to be

30 K. Hysteresis loop collected at 2K shows an interesting wasp-shape (inset to the **Figure 4b**), which occurs for materials with coexistence of components with contrasting coercivities. In our case the exchange bias was not observed, hence interaction with the impurity phase could be excluded. For this reason, this could be attributed to the distribution of magnetic domain sizes, which is likely for heavily frustrated systems.

In contrast to the previous cases, the CW behavior of $La_4Co_4Bi$ (**Figure 4c**) could not be observed due to the antiferromagnetic impurity phase $La_2Co_3$ ($T_N$ = 315 K [83]). However, at 50 K irreversibility in FC and ZFC curves arises. As apparent the magnetic susceptibility at small fields as well as magnetization collected at 2 K in the magnetic field of 7 T are very small. The isothermal magnetization shows a small ferromagnetic-like contribution overlaid onto an antiferromagnetic signal. Owing to the saturation of the small hysteresis loop of 0.015 $\mu_B$ only, one may expect that this suggests non-magnetic (van Vleck paramagnetism) or spin glass properties of the $La_4Co_4Bi$.

Magnetic properties of compounds with triangular arrangements of magnetic atoms (hexagonal, pyrochlore or Kagomé lattices) are usually complex as magnetic frustration may favor second or further neighbors to play a crucial role in the RKKY exchange. This is the case for 4:4:1 family, which exhibits decorated Kagomé motifs built from Co atoms stacked within the *ac* plane (see **Figure 1**). The decoration by out-of-plane Co atoms may introduce additional Dzyaloshinskii-Moriya interaction, which favors complex non-collinear, modulated magnetic structures. Usually, cobalt compounds are ferromagnetic, as long as Co is the only magnetic atom in the lattice. Some exceptions are known mainly in the binary *R*-Co (*R* = rare earth) system [83, 84]. In light of the above, we suggest that the compounds do not exhibit magnetic ordering down to the lowest temperatures studied due to the complexity of the magnetic interactions.

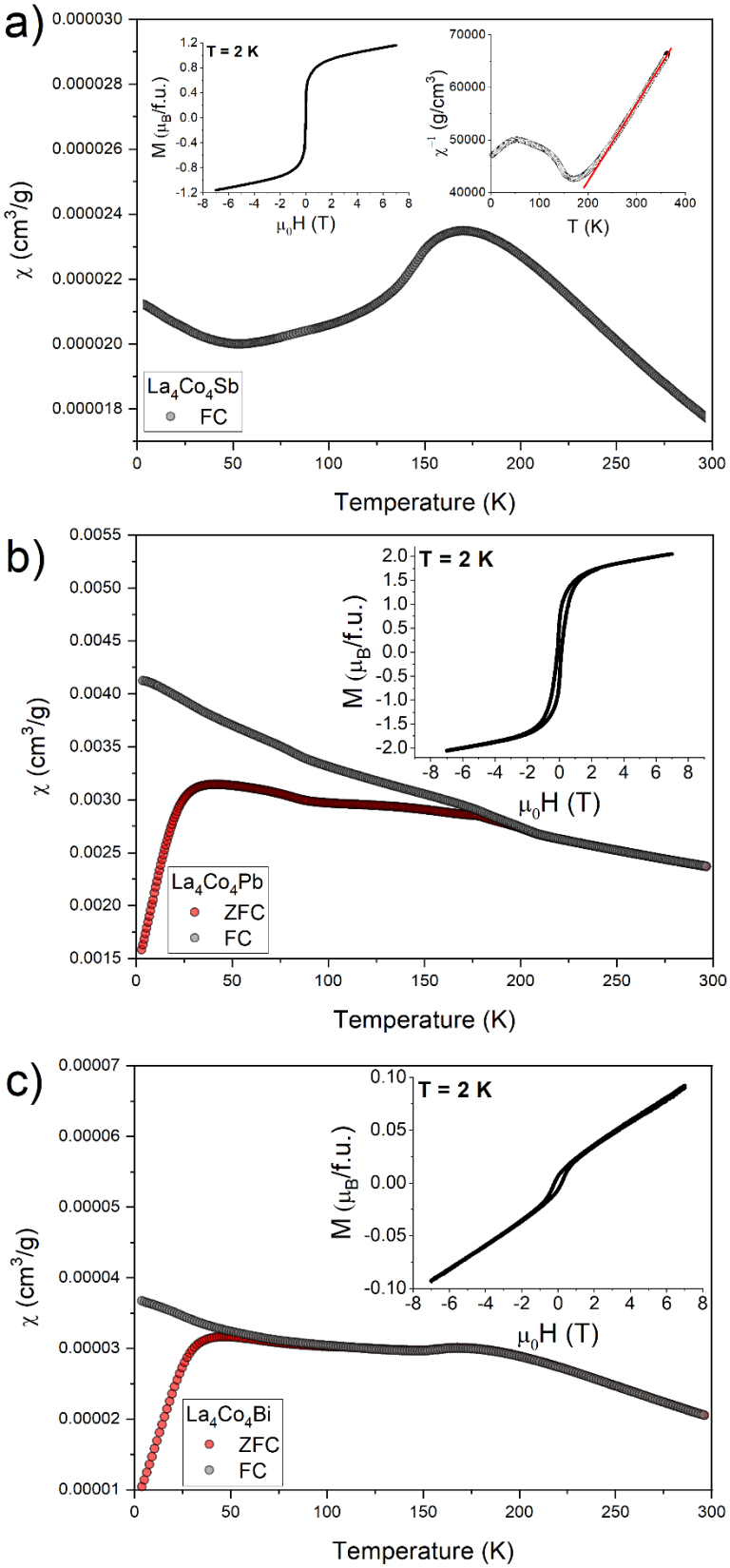


**Figure 4**. Magnetic properties of $La_4Co_4M$ with *M*=Sb (a), Pb (b), and Bi (c). Field-cooled (FC) and Zero field-cooled (ZFC) curves were measured in the field of 0.01 T, except for $La_4Co_4Sb$, where 5T magnetic field was used. Isothermal magnetization loops collected at 2 K are presented in the insets. For the $La_4Co_4Sb$ compound inverse susceptibility was plotted in the inset to part (a), along with the Curie-Weiss fit (red line).

For the $La_3Ni_3Al$ compound, the magnetic susceptibility shows no Curie-Weiss behavior, as well as the modified one, in the investigated temperature range (**Figure 5a**). The susceptibility shows a broad maximum at about 37 and 22 K for ZFC and FC curves, respectively. Additionally, small departure between the FC and ZFC curves can be noticed below roughly 250 K. However, the collected magnetization curves (inset to **Figure 5a**) show an extremely small signal. Measurements performed at higher magnetic fields of 5T revealed that the sample shows temperature independent behavior above 25 K. The discrepancy between low and high field data is a clear sign that the above-mentioned anomalous behavior originates from spurious phases. This is supported by isothermal magnetization curves, which shows small ferromagnetic signal with saturation of 0.005 $\mu_B$ only. It can be presumably associated with traces of pure nickel, hence, ferromagnetic precipitations. Taking above into account the sample can be classified as the van Vleck paramagnet.

For the $La_3Ni_3Ga$ alloy, the magnetic susceptibility shows temperature-independent behavior between 200–380 K with hysteresis loops typical of weak paramagnet with extremely small values of magnetic moment (**Figure 5b**). The low-temperature part of the susceptibility shows a small maximum at about 51 K, which is presumably related to the traces of the $La_2Ni_7$ impurity phase, which was reported to order antiferromagnetically at that temperature [85]. The measurements performed at higher magnetic fields did not reveal substantial changes, apart from flattering the curve above 100 K. Additionally, the inverse susceptibility does not follow the Curie-Weiss behavior, which suggests that the sample is van Vleck paramagnet, as well. Below 25 K the magnetic susceptibility shows some rise, which may originate from some traces of pure Ni precipitations at the grains boundaries, as the isothermal magnetization shows some small ferromagnetic component with the saturation moment less than 0.0007 $\mu_B$. For both compounds, the lack of the long-range magnetic ordering along with Curie-Weiss behavior is in agreement with electronic structure calculations discussed below.

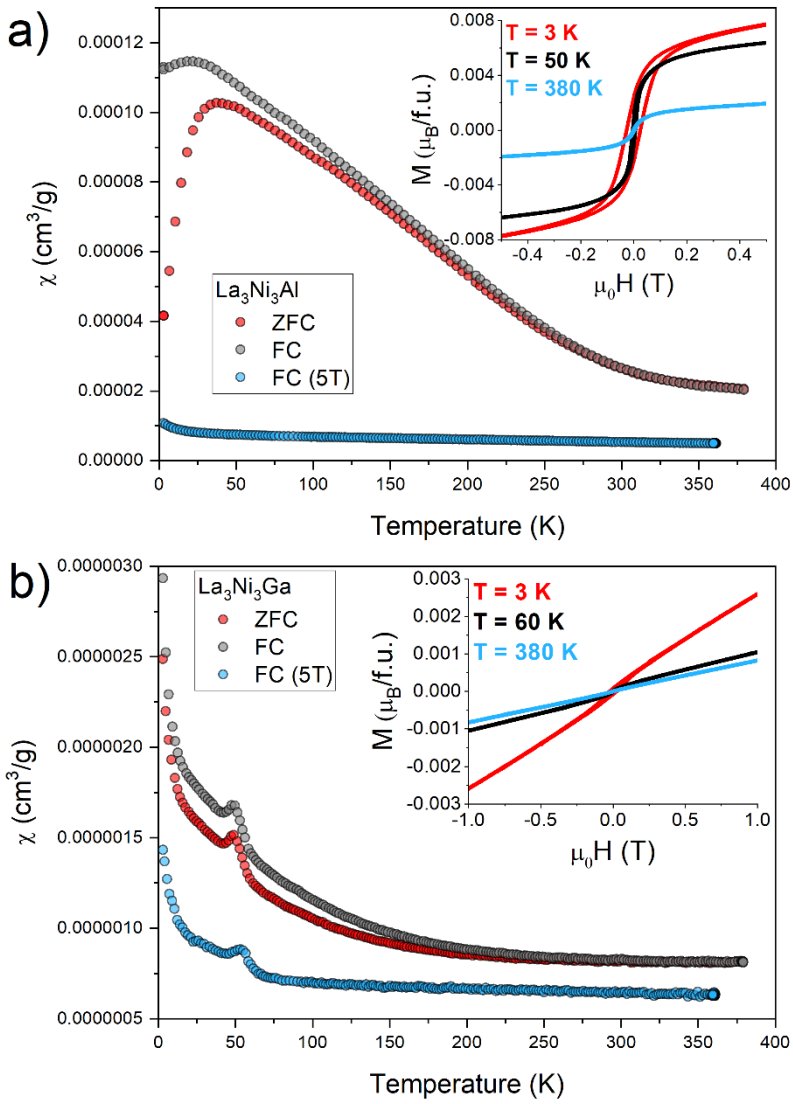


**Figure 5**. Magnetic properties of $La_3Ni_3Al$ (a) and $La_3Ni_3Ga$ (b). Zero field cooled (ZFC) curves were measured in a field of 0.01 T and 5 T. Inserts show isothermal magnetization curves measured at several temperatures.

*3.3 Electronic structures*

To gain a better understanding of the composition-structure-property relationships in the investigated compounds, band structure calculations have been performed. The initial sets of structural parameters for the selected $La_4Co_4M$ ($M$ = Bi, Sb and Pb) and $La_3Ni_3M$ ($M$ = Ga and Al) have been relaxed and the optimized data have been provided in **Table 3**. The optimized average volume is comparable to the experimental ones, with a small underestimation (usually not exceeding 1%), though not expected when using the PBE exchange and correlation functional.

**Table 3**. Relaxed cell parameters after DFT Calculation, Total magnetic moment, Heat of formation and average Bader charge by atom.

| Compound | SG | Cell Parameters | | | $V$/Å$^3$ | Magnetic Moment, $\mu_B$/at | $\Delta_f H$, kJ/mol | Bader charges | | |
|---|---|---|---|---|---|---|---|---|---|---|
| | | $a$/Å | $b$/Å | $c$/Å | | | | La | Co/Ni | $M$ |
| $La_4Co_4Bi$ | *Pbam* | 8.240 | 21.600 | 4.800 | 854.32 | 0.17 | -32.69 | 1.065 | -0.686 | -1.518 |
| $La_4Co_4Sb$ | *Pbam* | 8.312 | 21.838 | 4.646 | 843.33 | 0.20 | -41.57 | 1.098 | -0.692 | -1.622 |
| $La_4Co_4Pb$ | *Pbam* | 8.354 | 21.924 | 4.683 | 857.71 | 0.24 | -24.40 | 1.079 | -0.678 | -1.605 |
| $La_3Ni_3Ga$ | *Cmcm* | 4.177 | 10.533 | 13.699 | 602.71 | 0.00 | -42.16 | 1.043 | -0.886 | -0.469 |
| $La_3Ni_3Al$ | *Cmcm* | 4.150 | 10.642 | 13.756 | 607.52 | 0.00 | -39.94 | 1.026 | -1.185 | 0.478 |

Using spin relaxation, only the Co-based compounds converged to a distinguishable ferromagnetic ordering with a weak magnetic moment of about 0.2 $\mu_B$/at, mainly held by the Co atoms in 8*i* and 2*d* positions (0.9 $\mu_B$/at), with a small ferrimagnetic contribution from La. Several magnetic orders, such as antiferromagnetic, have been tested on the Ni-based compounds, all falling to a Pauli paramagnetic, within the pseudo-potential approximation. All these spin polarization results show a good agreement with the experimental measurement, where the Ni-based compounds hardly reveal any magnetic ordering. For the Co-based compound, as in the measurement, the calculation shows that the Co atoms hold the major magnetic contribution. The total moment is slightly different, which can be explained by the pseudopotential approximation used.

The electronic DOS is shown in **Figure 6**. For all compounds, a small structure around 6 to 8 eV below the Fermi level corresponds to the hybridized *sp* bands of the *M* element, while the valence structure is mainly composed of the 3*d* elements. The filling of these dense bands could be clarified with the Bader analysis, and the corresponding electronic charge transfer is given in **Table 3**. While La allows to give about 1 electron, the 3*d* element fills its bands by grabbing 0.7 electrons for Co and 0.9–1.2 for Ni. Since Ni reveals practically filled 3*d* bands in both spin directions, it serves as a good explanation for the absence of magnetism for both Ni-based compounds. It can be noted that the *s*-*p* elements such as Sb, Bi and Pb capture about 1.5 electrons thanks to their highest electronegativity, whereas Al, the worst electronegative, even gives electrons to the system, especially to fill the Ni-3*d* bands as explained earlier.

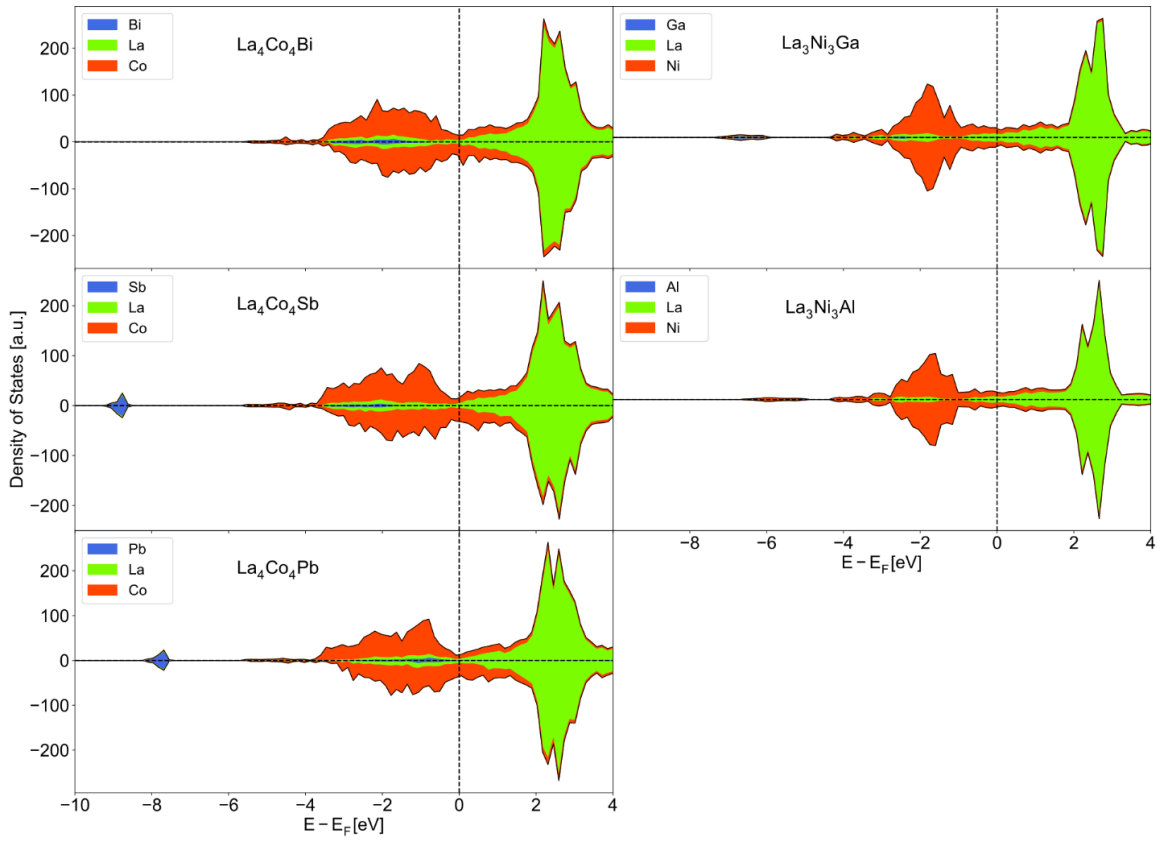


**Figure 6**. Electronic density of states with partial contribution of each atom for both spin directions of $La_4Co_4M$ (*M*=Bi, Sb, Pb) and $La_3Ni_3M$ (*M*=Ga, Al) compounds.

The heat of formation, $\Delta_f H$, for all compounds has been calculated and shows a value around -40 kJ/mol, as usual for the intermetallics of La with transition elements [86]. The mechanical stability has been studied in the harmonic approximation. As an example, the phonon dispersion curves of $La_4Co_4Bi$ and $La_3Ni_3Ga$ present no imaginary frequencies (**Figure 7**). The *M* element has acoustic branches in common with Co/Ni, while the heavier atom, La, vibrates at lower frequencies. The $La_4Co_4Bi$ presents a vibrational contribution center of the Bi, as the *s-p* element, located at lower frequencies compared with the Ga, due to the respective weight.

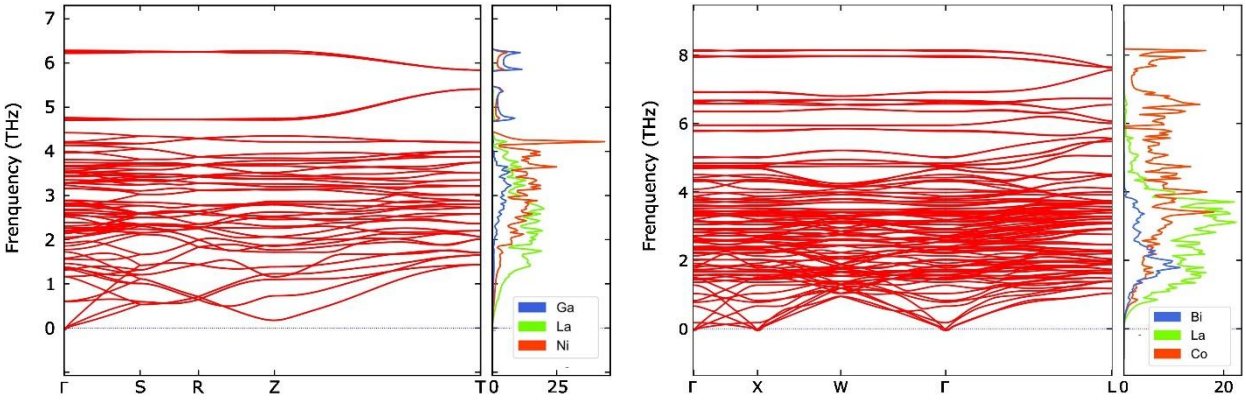


**Figure 7**. Phonon dispersion curves and associated DOS of $La_3Ni_3Ga$ (left) and $La_4Co_4Bi$ (right).

*3.4 Chemical Bonding*

Bonding analysis by the COHP method for $La_3Ni_3Ga$ and $La_4Co_4Sn$ as representative examples of the corresponding series (**Figures 8**, **9** and S4-6, **Table 4**) revealed plenty of common features, although compounds exhibit different composition-related structural and bonding motifs. The principal difference comes from the participation of the second anionic component. While in the crystal structure of 3:3:1 the *p* element is involved in the formation of the kagomé-like layers, in 4:4:1 it stays separately leading to the absence of heteroanionic contacts.

Ni-Ni contacts in the octagons are somewhat shorter compared to those in the $Ni_2Ga$ triangles and correspondingly show a higher bond population. The latter are naturally affected by strong heteroatomic Ni-Ga interactions. Weak antibonding contributions for the Ni-Ni pairs, especially longer ones, could be observed at 0.1-2 eV below $E_F$ due to possible repulsion between the filled *d* states [87-89]. With a little exception for those longer Ni-Ni contacts, all interactions are significantly bonding at the Fermi level. It is also worth noting La atoms participate actively in the covalent bonding interactions providing almost 60% of the total bonding population and even La-La interactions are not negligible (**Table 4**).

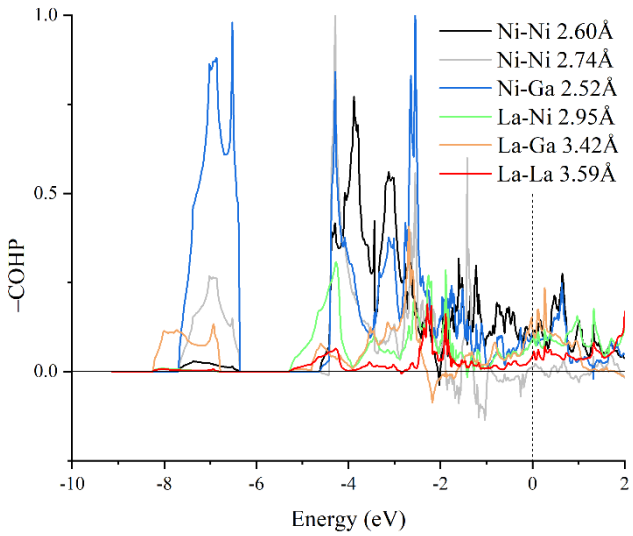


**Figure 8.** –COHP curves of the six types of bonds in the crystal structure of $La_3Ni_3Ga$. Only selected La-Ni, La-Ga and La-La bonds have been plotted for clarity purposes. The Fermi level is indicated by a dotted line.

Since Co-Sn interactions are not present in the crystal structure of $La_4Co_4Sn$, all interanionic interactions are represented by Co-Co bonds, although their total contribution is comparable to those of Ni-Ni and Ni-Ga together in $La_3Ni_3Ga$. Most of the interactions are non-bonding at the Fermi level. Some specific interactions reveal antibonding character particularly the Co-Co pairs within $Co_4$ tetrahedra, particularly those involving Co atoms capping triangles of the kagomé tiling. Interestingly, another Co-Co bond in the same tetrahedron outside the kagomé layer is the longest, the least populated and optimized at 0.5 eV below $E_F$, while the remaining Co-Co bonds

of the hexagons are always bonding. Similarly to $La_3Ni_3Ga$, La-Co and La-Sn contributions are significant (almost 50%) and significantly bonding below $E_F$, though their proportion is more steady (**Table 4**) due to the isolation of the Sn positions. La-La contributions in both structures are comparable as well.

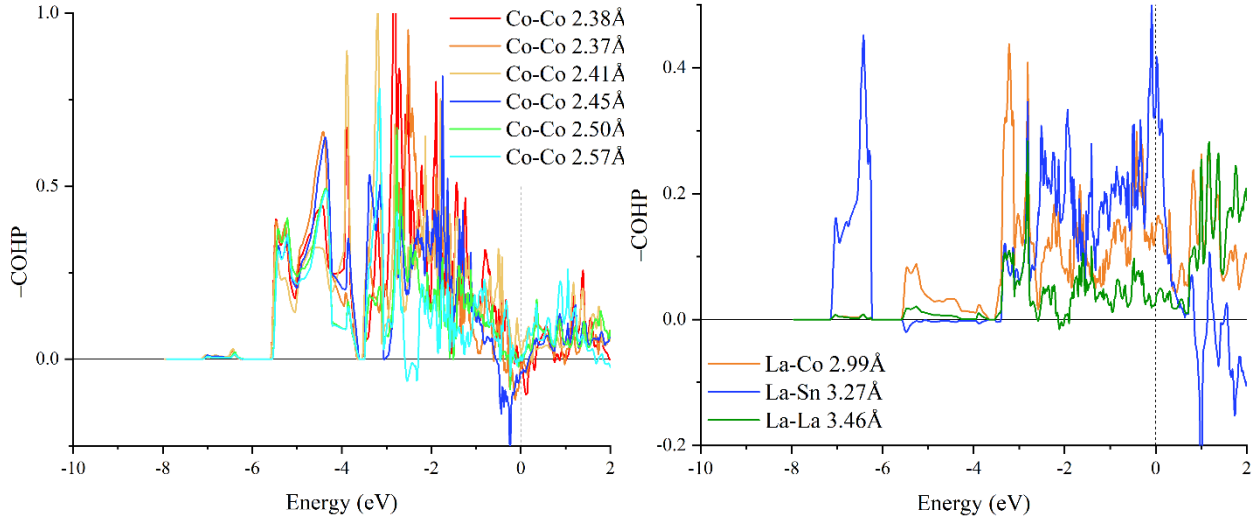


**Figure 9.** –COHP curves of (left) all Co-Co bonds and (right) three representative La-Co, La-Sn and La-La bonds in the crystal structure of $La_4Co_4Sn$. The Fermi levels are indicated by dotted lines.

**Table 4.** Bond length ranges, average –ICOHP values and total contributions to bonding interactions in $La_3Ni_3Ga$ and $La_4Co_4Sn$.

| Bond type | Length (Å) | –ICOHP | No./cell | –ICOHP | Contribution |
|---|---|---|---|---|---|
| | | | $La_3Ni_3Ga$ | | |
| Ga-Ni | 2.52 | 1.65 | 16 | 26.4 | 26.0 |
| Ni-Ni | 2.60 | 1.10 | 12 | 13.2 | 13.0 |
| | 2.74 | 0.69 | 4 | 2.8 | 2.7 |
| La-Ni | 2.95 | 0.41 | 8 | 3.3 | 3.2 |
| | 3.01–3.06 | 0.48 | 40 | 19.2 | 18.9 |
| | 3.10–3.17 | 0.45 | 32 | 14.3 | 14.1 |
| | 3.19 | 0.56 | 4 | 2.2 | 2.2 |
| La-Ga | 3.28 | 0.45 | 12 | 5.4 | 5.3 |
| | 3.41–3.42 | 0.37 | 24 | 8.8 | 8.7 |
| La-La | 3.59 | 0.14 | 16 | 2.2 | 2.2 |
| | 3.70 | 0.20 | 16 | 3.2 | 3.1 |
| | 4.00 | 0.14 | 4 | 0.6 | 0.6 |
| | | | $La_4Co_4Sn$ | | |
| Co-Co | 2.37–2.41 | 1.44 | 16 | 23.0 | 20.4 |
| | 2.45 | 1.29 | 12 | 15.4 | 13.6 |
| | 2.50–2.57 | 0.99 | 12 | 11.9 | 10.5 |
| La-Co | 2.90 | 0.76 | 12 | 9.1 | 8.1 |
| | 2.93–3.05 | 0.43 | 44 | 18.9 | 16.7 |
| | 3.29 | 0.28 | 8 | 2.2 | 2.0 |
| La-Sn | 3.27 | 0.79 | 4 | 3.2 | 2.8 |
| | 3.36–3.42 | 0.71 | 24 | 17.0 | 15.1 |
| | 3.53 | 0.62 | 8 | 5.0 | 4.4 |
| La-La | 3.46 | 0.18 | 4 | 0.7 | 0.6 |

| | | | | | |
|---|---|---|---|---|---|
| | 3.70–3.78 | 0.14 | 20 | 2.8 | 2.5 |
| | 3.80–4.02 | 0.16 | 24 | 3.8 | 3.4 |

# 4. Conclusions

Two isostructural series, $La_4Co_4M$ ($M$ = Sn, Sb, Te, Pb, Bi) and $La_3Ni_3M$ ($M$ = Al, Ga) have been synthesized. Both series are characterized by interesting variations of the semiregular tilings of the corrugated anionic layers combined with predominantly cationic zigzag motifs. The layers in $La_4Co_4M$ are of augmented Kagomé type with a minimal degree of corrugation, while those in $La_3Ni_3M$ have a more complex tiling ($3^28^2$) and a more significant degree of corrugation. In some sense larger ($8^2$) fragments exist of two truncated hexagons and the corrugation is required to keep the optimized Co-Co-Co bonding angles (~120°) within the polyanionic layer. The discovery of the $La_4Co_4M$ series brought us to the fact that such types of compounds can be obtained with 'antagonistic pairs' *i.e*. Co-Pb or Co-Bi. As for the $La_3Ni_3M$ compounds, it is only the second observation of such a structure containing La and the first one within *R*–Ni–*M* (*R*= rare earth element, *M* = Ga and Al) systems.

Magnetic characterization has been performed for both series. For $La_4Co_4M$ compounds, we were unable to prove long-range magnetic ordering due to strong magnetism from impurity phases. Only for the $La_4Co_4Sb$, complex antiferromagnetic ordering below 170 K was suggested. However, it seems that the other compounds show rather weak, frustrated magnetism, if any. No magnetic ordering in the $La_3Ni_3M$ series was evidenced. The magnetic susceptibility was found to be temperature independent with no Curie-Weiss behavior, which is likely a sign of van Vleck paramagnetism. From the electronic structure study, the partial charge transfer from La to the other elements explains the filling of the 3*d*-Ni bands and the corresponding absence of magnetism for Ni-based compounds.

The electronic densities of states of $La_4Co_4M$ show extensive overlaps, large mostly Co-*d* states dominating at 0–4 eV below the Fermi level and local minima at $E_F$. Predominantly *M*-*p* states could be observed at -8 eV or below. As for $La_3Ni_3M$ large Ni-*d* states are less broad dominating at 1.5–2.5 eV, while the *M*-*p* states are located at 6–7 eV below $E_F$. The bonding picture in both series is qualitatively and quantitatively similar showing enhanced contribution from the La pairs. Even though heteroanionic pairs could not be observed in $La_4Co_4M$ total contribution from both anionic pairs in $La_3Ni_3M$ is equal to the Co-Co contribution. Similarly, contributions from the La-La pairs are not negligible in both compounds giving ~6% in total.

**Acknowledgments**

We acknowledge Myfab Uppsala for providing facilities. Myfab is funded by the Swedish Research Council as a national research infrastructure. VSh and MS acknowledges financial support from the Foundation for Strategic Research (SSF), grant #EM16-0039, as well as from

ÅForsk, grant # 21-196, is gratefully acknowledged. DFT calculations were performed using HPC resources from GENCI–CINES (Grant A0060906175). AK acknowledges support from the Swedish Strategic Research Council (SSF UKR22-0050). AVM acknowledges DFF (Danmarks Frie Forskningsfind) for support.

# References

[1] A. Ovchinnikov, V. Smetana, A.-V. Mudring, Metallic alloys at the edge of complexity: structural aspects, chemical bonding and physical properties, J. Phys.: Condens. Matter 32 (2020) 243002. https://doi.org/10.1088/1361-648x/ab6b87

[2] G.J. Miller, M.W. Schmidt, F. Wang, T.-S. You, in Quantitative Advances in the Zintl–Klemm Formalism, T.F. Fässler (Ed.), Zintl Phases: Principles and Recent Developments, Springer Berlin Heidelberg, Berlin, Heidelberg, 2011, pp. 1-55.

[3] V. Smetana, M. Rhodehouse, G. Meyer, A.-V. Mudring, Gold polar intermetallics: structural versatility through exclusive bonding motifs, Acc. Chem. Res. 50 (2017) 2633-2641. https://doi.org/10.1021/acs.accounts.7b00316

[4] Q. Lin, G.J. Miller, Electron-Poor Polar Intermetallics: Complex Structures, Novel Clusters, and Intriguing Bonding with Pronounced Electron Delocalization, Acc. Chem. Res. 51 (2018) 49-58. https://doi.org/10.1021/acs.accounts.7b00488

[5] K.S. Kumar, in Intermetallics: Silicides, F.G. Caballero (Ed.), Encyclopedia of Materials: Metals and Alloys, Elsevier, Oxford, 2001, pp. 335-338.

[6] R. Pöttgen, Stannides and Intermetallic Tin Compounds – Fundamentals and Applications, Z. Naturforsch. B 61 (2006) 677-698. https://doi.org/10.1515/znb-2006-0607

[7] S. Klenner, R. Pöttgen, in Chapter 312 - Rare earth transition metal plumbides – An update, J.-C.G. Bünzli, V.K. Pecharsky (Eds.), Handbook on the Physics and Chemistry of Rare Earths, Elsevier, 2020, pp. 1-44.

[8] A. Mar, in Chapter 227 Bismuthides, K.A. Gschneidner, J.-C.G. Bunzli, V.K. Pecharsky (Eds.), Handbook on the Physics and Chemistry of Rare Earths, Elsevier, 2006, pp. 1-82.

[9] S. Singh, R. Kumar, Superconducting Properties of $LaSn_3$ Under Positive Hydrostatic Pressure, J. Supercond. Nov. Magn. 32 (2019) 3431-3436. https://doi.org/10.1007/s10948-019-5134-0

[10] F. Weitzer, K. Hiebl, P. Rogl, Crystal-Chemistry and Magnetism of Neodymium Stannides Including Compounds of the Structural Series $RE_nSn_{3n-2}$, J. Solid State Chem. 98 (1992) 291-300. https://doi.org/10.1016/S0022-4596(05)80237-3

[11] B.T. Matthias, T.H. Geballe, V.B. Compton, Superconductivity, Reviews of Modern Physics 35 (1963) 1-22. https://doi.org/10.1103/RevModPhys.35.1

[12] Z.W. He, R.J. Huang, K.Y. Zhou, Y. Liu, S.B. Guo, Y.Z. Song, Z.N. Guo, S.X. Hu, L.H. He, Q.Z. Huang, L.F. Li, J.Y. Zhang, S.G. Wang, J.G. Guo, X.R. Xing, J. Chen, Superconductivity in Co-Layered LaCoSi, Inorg. Chem. 60 (2021) 6157-6161. https://doi.org/10.1021/acs.inorgchem.1c00699

[13] Y. Gong, J. Wu, M. Kitano, J. Wang, T.-N. Ye, J. Li, Y. Kobayashi, K. Kishida, H. Abe, Y. Niwa, H. Yang, T. Tada, H. Hosono, Ternary intermetallic LaCoSi as a catalyst for $N_2$ activation, Nature Catalysis 1 (2018) 178-185. https://doi.org/10.1038/s41929-017-0022-0

[14] S.P. Yatsenko, R.E. Gladyshevskii, O.M. Sitschewitsch, V.K. Belsky, A.A. Semyannikov, Y.N. Hryn, Y.P. Yarmolyuk, Kristallstruktur von $Gd_3Ga_2$ und isotypen Verbindungen, J. Less Common Met. 115 (1986) 17-22. https://doi.org/10.1016/0022-5088(86)90367-X

[15] F. Weitzer, A. Leithejasper, P. Rogl, K. Hiebl, H. Noel, G. Wiesinger, W. Steiner, Magnetism of (Fe,Co)-Based Alloys with the $La_6Co_{11}Ga_3$-Type, J. Solid State Chem. 104 (1993) 368-376. https://doi.org/10.1006/jssc.1993.1172

[16] N. Bestaoui, P.S. Herle, J.D. Corbett, New Ternary Lanthanide Transition-Metal Tellurides: $Dy_6MTe_2$, $M$=Fe, Co, Ni, J. Solid State Chem. 155 (2000) 9-14. https://doi.org/10.1006/jssc.2000.8880

[17] A.M. Guloy, J.D. Corbett, Exploration of the Interstitial Derivatives of $La_5Pb_3$ ($Mn_5Si_3$-Type), J. Solid State Chem. 109 (1994) 352-358. https://doi.org/10.1006/jssc.1994.1114

[18] L.D. Gulay, Y.M. Kalychak, M. Wolcyrz, K. Lukaszewicz, Crystal structure of $R_{12}Ni_6Pb$ ($R$=Y, La, Pr, Nd, Sm, Gd, Tb, Dy, Ho) and $R_{12}Co_6Pb$ ($R$=Y, La, Pr, Nd, Sm, Gd) compounds, J. Alloys Compd. 311 (2000) 238-240. https://doi.org/10.1016/S0925-8388(00)01115-4

[19] A. Leithejasper, P. Rogl, The Crystal-Structure of $NdFe_{1-x}Sb_2$ and Isotypic Compounds *RE*$(Fe, Co)_{1-x}Sb_2$ (*RE*=La, Ce, Pr, Sm, Gd), J. Alloys Compd. 203 (1994) 133-136. https://doi.org/10.1016/0925-8388(94)90723-4
[20] W.Z. Cai, L.M. Wu, L.H. Li, L. Chen, Syntheses, Structures, and Theoretical Studies of New Ternary Antimonides beta-*RE*$CoSb_3$ (*RE* = La-Nd, Sm), Eur. J. Inorg. Chem. 2 (2009) 230-237. https://doi.org/10.1002/ejic.200800836
[21] J.L. Mi, M. Christensen, E. Nishibori, V. Kuznetsov, D.M. Rowe, B.B. Iversen, Multitemperature synchrotron powder diffraction and thermoelectric properties of the skutterudite $La_{0.1}Co_4Sb_{12}$, J. Appl. Phys. 107 (2010) 113507. https://doi.org/10.1063/1.3428435
[22] M. Pani, P. Manfrinetti, A. Palenzona, S.K. Dhar, S. Singh, Synthesis, crystal structure, magnetic and transport properties of the new intermetallic compounds $R_4Co_2Sn_5$ (*R*=La, Ce), J. Alloys Compd. 299 (2000) 39-44. https://doi.org/10.1016/S0925-8388(99)00789-6
[23] Y. Mudryk, P. Manfrinetti, V. Smetana, J. Liu, M.L. Fornasini, A. Provino, V.K. Pecharsky, G.J. Miller, K.A. Gschneidner, Structural disorder and magnetism in rare-earth (*R*) $R_{117}Co_{54+x}Sn_{112\pm y}$, J. Alloys Compd. 557 (2013) 252-260. https://doi.org/10.1016/j.jallcom.2012.12.137
[24] W. Dörrscheidt, H. Schäfer, Darstellung und kristallstruktur von $BaPdSn_3$, $SrPdSn_3$ und $La_3Co_2Sn_7$, J. Less Common Met. 70 (1980) P1-P10. https://doi.org/10.1016/0022-5088(80)90282-9
[25] G.P. Espinosa, A.S. Cooper, H. Barz, Isomorphs of the Superconducting-Magnetic Ternary Stannides, Mater. Res. Bull. 17 (1982) 963-969. https://doi.org/10.1016/0025-5408(82)90121-0
[26] Y. Grin, Y. Yarmolyuk, The crystal structure of the compounds $La_3Ga_2Ni_4$ and $Pr_3Ga_2Ni_4$, Sov. Phys. Crystallogr. 25 (1980) 353-355.
[27] V. Romaka, Y. Grin, Y. Yarmolyuk, O. Zarechnyuk, R. Skolozdra, Magnetic and crystallographic parameters of $R_2Ni_2Ga$ and $R_2Ni_2Al$ compounds, Phys. Met. Metallogr. 54 (1982) 58-64.
[28] S. Xie, J. Liang, Phase-Equilibria in $LaNi_{5-x}Ga_x$ ($x \leq 4$) System and Their Hydrogen Absorption Properties, Kexue Tongbao 29 (1984) 29-34.
[29] Y. Prots, L. Vasylechko, W. Carrillo-Cabrera, C. Drathen, M. Coduri, D. Kaczorowski, U. Burkhardt, Y. Grin, Compositional evolution of the $NaZn_{13}$ structure motif in the systems La-Ni-Ga and Ce-Ni-Ga, Dalton Trans. 47 (2018) 12951-12963. https://doi.org/10.1039/c8dt02273a
[30] Y. Grin, Y. Yarmolyuk, Crystal structure of the $RGa_2Ni$ compounds (*R*= La, Ce, Pr, Nd, Sm, Gd), Dopov. Akad. Nauk Ukr. RSR, Ser. A 3 (1982) 69-72.
[31] O. Sichevich, S. Kim, L. Vasylechko, Y. Grin, Y. Yarmolyuk, Phases with type $BaZn_5$ structure in the ternary systems (Ca,La,Eu)-(Co,Ni)-Ga, Russ. Metall. 4 (1986) 209-212.
[32] J.Y. Cho, J.N. Millican, C. Capan, D.A. Sokolov, M. Moldovan, A.B. Karki, D.P. Young, M.C. Aronson, J.Y. Chan, Crystal Growth, Structure, and Physical Properties of $Ln_2MGa_{12}$ (*Ln* = La, Ce; *M* = Ni, Cu), Chem. Mater. 20 (2008) 6116-6123. https://doi.org/10.1021/cm801693t
[33] Y. Yarmolyuk, Y. Grin, I. Rozhdestvenskaya, O. Usov, A. Kuz'min, V. Bruskov, E. Gladyshevskii, Crystal chemistry of series of inhomogeneous linear structures. III. The crystal structures of $Ce_2Ga_{10}Ni$ and $La_2Ga_{10}Ni$, Kristallografiya 27 (1982) 999-1001.
[34] J.C. Achard, F. Givord, A. Percheronguegan, J.L. Soubeyroux, F. Tasset, Neutron Study of Al or Mn Substituted $LaNi_5$ Hydrogen Sponges, J Phys. Colloques 40 (1979) 218-220. https://doi.org/10.1051/jphyscol:1979582
[35] A. Leineweber, H. Nitsche, $La_5Al_3Ni_2$ - an intermetallic phase observed upon crystallization of $La_{50}Al_{25}Ni_{25}$ metallic glass, Z. Anorg. Allg. Chem. 632 (2006) 553-558. https://doi.org/10.1002/zaac.200500387
[36] N. Zaremba, Y. Schepilov, G. Nychyporuk, V. Hlukhyy, V. Pavlyuk, $La_3Ni_4Al_2$: a new layered aluminide, Z. Kristallogr. Cryst. Mat. 234 (2019) 581-586. https://doi.org/10.1515/zkri-2019-0011
[37] G. Cordier, G. Dörsam, R. Kniep, New intermediate phases in the ternary systems rare earth-transition element-aluminium, J. Magn. Magn. Mater. 76-77 (1988) 653-654. https://doi.org/10.1016/0304-8853(88)90517-3
[38] M. Radzieowski, F. Stegemann, C. Doerenkamp, S.F. Matar, H. Eckert, C. Dosche, G. Wittstock, O. Janka, Correlations of Crystal and Electronic Structure via NMR and X-ray Photoelectron Spectroscopies in the *RETM*$Al_2$ (*RE* = Sc, Y, La-Nd, Sm, Gd-Tm, Lu; *TM* = Ni, Pd, Pt) Series, Inorg Chem 58 (2019) 7010-7025. https://doi.org/10.1021/acs.inorgchem.9b00648
[39] R.E. Gladyshevskii, K. Cenzual, E. Parthe, $LaNi_2Al_3$, a Ternary Substitution Variant of the Orthorhombic $BaZn_5$ Type, Acta Crystallogr B 48 (1992) 389-392. https://doi.org/10.1107/S0108768192001502
[40] Y. Yarmolyuk, R. Rykhal', L. Akselrud, O. Zarechnyuk, Crystal structure of the $PrNi_2Al_5$ compound and its analogs, Dopov. Akad. Nauk Ukr. RSR, Ser. A 9 (1981) 86-90.

[41] D. Gout, E. Benbow, O. Gourdon, G.J. Miller, Composition-structure relationships in polar intermetallics: Experimental and theoretical studies of $LaNi_{1+x}Al_{6-x}$ ($x$=0.44), Inorg. Chem. 43 (2004) 4604-4609. https://doi.org/10.1021/ic0497331
[42] D. Gout, T.J. Barker, O. Gourdon, G.J. Miller, A new superstructure for the $BaAl_4$-structure type: An experimental and theoretical study of $La_2NiAl_7$, Chem. Mater. 17 (2005) 3661-3667. https://doi.org/10.1021/cm050513a
[43] F. Serrano-Sanchez, J. Prado-Gonjal, N.M. Nemes, N. Biskup, M. Varela, O.J. Dura, J.L. Martinez, M.T. Fernandez-Diaz, F. Fauth, J.A. Alonso, Low thermal conductivity in La-filled cobalt antimonide skutterudites with an inhomogeneous filling factor prepared under high-pressure conditions, J. Mater. Chem. A 6 (2018) 118-126. https://doi.org/10.1039/c7ta08545a
[44] Z. Blazina, A. Drasner, On the structural and thermodynamic properties of the *RE*$Ni_4Ga$-hydrogen (*RE*=La, Ce, Nd and Sm) systems, J. Phys.: Condens. Matter 10 (1998) 4777-4783. https://doi.org/10.1088/0953-8984/10/22/006
[45] H. Diaz, A. Percheron-Guégan, J.C. Achard, C. Chatillon, J.C. Mathieu, Thermodynamic and structural properties of $LaNi_{5-y}Al_y$ compounds and their related hydrides, Int. J. Hydrogen Energy 4 (1979) 445-454. https://doi.org/10.1016/0360-3199(79)90104-6
[46] M. Afshari, Structural and Magnetic Properties of $LaNi_5$ and $LaNi_{3.94}Al_{1.06}$ Alloys, Before and After Hydrogenation, J. Supercond. Nov. Magn. 30 (2017) 2255-2259. https://doi.org/10.1007/s10948-017-4045-1
[47] J. Tang, L. Li, C.J. Oconnor, Y.S. Lee, Strongly Enhanced Paramagnetism in $CeNi_{5-x}Ga_x$ and $LaNi_3Ga_2$, J. Alloys Compd. 207 (1994) 241-244. https://doi.org/10.1016/0925-8388(94)90212-7
[48] Y. Zhang, Review of the structural, magnetic and magnetocaloric properties in ternary rare earth $RE_2T_2X$ type intermetallic compounds, J. Alloys Compd. 787 (2019) 1173-1186. https://doi.org/10.1016/j.jallcom.2019.02.175
[49] Y.N. Grin, K. Hiebl, P. Rogl, H. Noël, Magnetism and structural chemistry of ternary gallides *RE*$Ni_xGa_{4-x}$ (*RE*=La, Ce, Pr, Nd, Sm, Gd, Tb)and $LaCo_{0.5}Ga_{3.5}$, J. Less Common Met. 162 (1990) 361-369. https://doi.org/10.1016/0022-5088(90)90351-J
[50] G. Bruzzone, M. Ferretti, F. Merlo, G. L. Olcese, Structural, magnetic and hydrogenation properties of $RNiAl_2$ ternary compounds, Lanthanide Actinide Res. 1 (1986) 153-161.
[51] P.C. Canfield, New materials physics, Rep. Prog. Phys. 83 (2020) 016501. https://doi.org/10.1088/1361-6633/ab514b
[52] H.M. Rietveld, A profile refinement method for nuclear and magnetic structures, J. Appl. Crystallogr. 2 (1969) 65-71. https://doi.org/10.1107/S0021889869006558
[53] A. Coelho, TOPAS and TOPAS-Academic: an optimization program integrating computer algebra and crystallographic objects written in C++, J. Appl. Crystallogr. 51 (2018) 210-218. https://doi.org/doi:10.1107/S1600576718000183
[54] APEX3 and SAINT. Bruker AXS Inc., Madison, Wisconsin, USA.
[55] L. Krause, R. Herbst-Irmer, D. Stalke, An empirical correction for the influence of low-energy contamination, J. Appl. Crystallogr. 48 (2015) 1907-1913. https://doi.org/10.1107/S1600576715020440
[56] G. Sheldrick, SHELXT - Integrated space-group and crystal-structure determination, Acta Crystallogr. Sect. A 71 (2015) 3-8. https://doi.org/10.1107/S2053273314026370
[57] G. Sheldrick, Crystal structure refinement with SHELXL, Acta Crystallogr. Sect. C: Struct. Chem. 71 (2015) 3-8. https://doi.org/10.1107/S2053229614024218
[58] V. Shtender, V. Smetana, J.C. Crivello, L. Gondek, J. Przewozznik, A.V. Mudring, M. Sahlberg, Honeycomb Constructs in the La-Ni Intermetallics: Controlling Dimensionality via Element Substitution, Inorg. Chem. 62 (2023) 14843-14851. https://doi.org/10.1021/acs.inorgchem.3c00502
[59] G. Kresse, D. Joubert, From ultrasoft pseudopotentials to the projector augmented-wave method, Phys. Rev. B 59 (1999) 1758-1775. https://doi.org/10.1103/PhysRevB.59.1758
[60] G. Kresse, J. Furthmüller, Efficient iterative schemes for ab initio total-energy calculations using a plane-wave basis set, Phys. Rev. B 54 (1996) 11169-11186.
[61] J.P. Perdew, K. Burke, M. Ernzerhof, Generalized gradient approximation made simple, Phys. Rev. Lett. 78 (1997) 1396-1396. https://doi.org/10.1103/PhysRevLett.78.1396
[62] V.L. Deringer, C. Goerens, M. Esters, R. Dronskowski, B.P.T. Fokwa, Chemical Modeling of Mixed Occupations and Site Preferences in Anisotropic Crystal Structures: Case of Complex Intermetallic Borides, Inorg. Chem. 51 (2012) 5677-5685. https://doi.org/10.1021/ic300023t
[63] A. Togo, F. Oba, I. Tanaka, First-principles calculations of the ferroelastic transition between rutile-type and $CaCl_2$-type $SiO_2$ at high pressures, Phys. Rev. B 78 (2008). https://doi.org/10.1103/PhysRevB.78.134106

[64] G. Henkelman, A. Arnaldsson, H. Jonsson, A fast and robust algorithm for Bader decomposition of charge density, Comput. Mater. Sci. 36 (2006) 354-360. https://doi.org/10.1016/j.commatsci.2005.04.010
[65] O.Y. Oleksyn, O.I. Bodak, Crystal-Structure of $R_3Ge_4$ Compounds (*R*= Er, Ho, Tm, Lu), J. Alloys Compd. 210 (1994) 19-21. https://doi.org/10.1016/0925-8388(94)90108-2
[66] D. Grilli, V. Smetana, S.J. Ahmed, V. Shtender, M. Pani, P. Manfrinetti, A.-V. Mudring, $La_{n(n+1)+x}Ni_{n(n+5)+y}Si_{(n+1)(n+2)-z}$: A Symmetric Mirror Homologous Series in the La–Ni–Si System, Inorg. Chem. 62 (2023) 10736-10742. https://doi.org/10.1021/acs.inorgchem.3c01194
[67] Y.M. Prots, W. Jeitschko, Lanthanum nickel silicides with the general formula $La_{(n+l)(n+2)}Ni_{n(n-1)+2}Si_{n(n+1)}$ and other series of hexagonal structures with metal : metalloid ratios close to 2:1, Inorg. Chem. 37 (1998) 5431-5438. https://doi.org/10.1021/ic980397w
[68] B. Cordero, V. Gomez, A.E. Platero-Prats, M. Reves, J. Echeverria, E. Cremades, F. Barragan, S. Alvarez, Covalent radii revisited, Dalton Trans. (2008) 2832-2838. https://doi.org/10.1039/B801115J
[69] R.E. Gladyshevskii, Y. Grin, Y.P. Yarmolyuk, Compounds of the $Mo_2NiB_2$ structure type in the systems *R*-Ga-Co (*R*= Nd, Sm, Gd, Tb, Dy Ho, Er, Tm, Y), Visn. Lviv. Derzh. Univ., Ser. Khim. 23 (1981) 26-30.
[70] E.I. Gladyshevskii, Y.P. Yarmolyuk, Y. Grin, Structures of ternary gallides of rare-earth metals-members of the homologous series $R_mR'_{3m+2n}X_n$ and $R_{m+n}R'_nX_{m+n}$, Dop. Akad. Nauk Ukrainy RSR, Seriya A 40 (1978) 855-858.
[71] P. Solokha, S. De Negri, A. Saccone, V. Pavlyuk, J.C. Tedenac, Crystal structure investigation of *RE*-Ni-Zn ternary compounds (*RE*=La, Ce, Tb), Z. Anorg. Allg. Chem. 633 (2007) 482-489. https://doi.org/10.1002/zaac.200600310
[72] S.K. Pati, C.N.R. Rao, Kagome network compounds and their novel magnetic properties, Chem. Commun. (2008) 4683-4693. https://doi.org/10.1039/B807207H
[73] K. Zhao, H. Deng, H. Chen, K.A. Ross, V. Petříček, G. Günther, M. Russina, V. Hutanu, P. Gegenwart, Realization of the kagome spin ice state in a frustrated intermetallic compound, Science 367 (2020) 1218-1223. https://doi.org/10.1126/science.aaw1666
[74] L. Ye, M. Kang, J. Liu, F. von Cube, C.R. Wicker, T. Suzuki, C. Jozwiak, A. Bostwick, E. Rotenberg, D.C. Bell, L. Fu, R. Comin, J.G. Checkelsky, Massive Dirac fermions in a ferromagnetic kagome metal, Nature 555 (2018) 638-642. https://doi.org/10.1038/nature25987
[75] Y. Wang, G.T. McCandless, X. Wang, K. Thanabalasingam, H. Wu, D. Bouwmeester, H.S.J. van der Zant, M.N. Ali, J.Y. Chan, Electronic Properties and Phase Transition in the Kagome Metal $Yb_{0.5}Co_3Ge_3$, Chem. Mater. 34 (2022) 7337-7343. https://doi.org/10.1021/acs.chemmater.2c01309
[76] X. Zhang, Z. Liu, Q. Cui, Q. Guo, N. Wang, L. Shi, H. Zhang, W. Wang, X. Dong, J. Sun, Z. Dun, J. Cheng, Electronic and magnetic properties of intermetallic kagome magnets $RV_6Sn_6$ (*R*=Tb-Tm), Physical Review Materials 6 (2022) 105001. https://doi.org/10.1103/PhysRevMaterials.6.105001
[77] S. Klenner, M.K. Reimann, R. Pöttgen, A europium kagome lattice in the solid solution $Eu_{3-x}Sr_xPt_4Zn_{12}$ – first zinc representatives of the $Gd_3Ru_4Al_{12}$ type, Z. Kristallogr. Cryst. Mat. 236 (2021) 215-223. https://doi.org/doi:10.1515/zkri-2021-2041
[78] K.H.J. Buschow, W.A.J.J. Velge, Phase relations and intermetallic compounds in the lanthanum-cobalt system, J. Less Common Met. 13 (1967) 11-17. https://doi.org/10.1016/0022-5088(67)90042-2
[79] I. Bigun, V. Smetana, Y. Mudryk, I. Hlova, M. Dzevenko, L. Havela, Y. Kalychak, V. Pecharsky, A.-V. Mudring, $EuNi_5InH_{1.5-x}$ ($x$ = 0–1.5): hydrogen induced structural and magnetic transitions, J. Mater. Chem. C 5 (2017) 2994-3006. https://doi.org/10.1039/C7TC00121E
[80] I. Bigun, S. Steinberg, V. Smetana, Y. Mudryk, Y. Kalychak, L. Havela, V. Pecharsky, A.-V. Mudring, Magnetocaloric Behavior in Ternary Europium Indides $EuT_5In$: Probing the Design Capability of First-Principles-Based Methods on the Multifaceted Magnetic Materials, Chem. Mater. 29 (2017) 2599-2614. https://doi.org/10.1021/acs.chemmater.6b04782
[81] Y. Grin, R.E. Gladyshevskii, A.N. Sobolev, Y.P. Yarmolyuk, Crystal chemistry of series of inhomogeneous linear structures. VII. The crystal structure of the compounds $Y_{2m+2n}Ga_{2n}Co_{2m+2n}$, Kristallografiya 29 (1984) 531-533.
[82] V.V. Shtender, V.V. Pavlyuk, O.Y. Zelinska, W. Nitek, V. Paul-Boncour, G.S. Dmytriv, W. Łasocha, I.Y. Zavaliy, The Y–Mg–Co ternary system: alloys synthesis, phase diagram at 500 °C and crystal structure of the new compounds, J. Alloys Compd. 812 (2020) 152072. https://doi.org/10.1016/j.jallcom.2019.152072
[83] D. Gignoux, R. Lemaire, R. Mendia-Monterroso, J.M. Moreau, J. Schweizer, Antiferromagnetism in the La-Co system, Physica B+C 130 (1985) 376-378. https://doi.org/10.1016/0378-4363(85)90261-X
[84] Y. Shi, D.S. Parker, E.S. Choi, K.P. Devlin, L. Yin, J. Zhao, P. Klavins, S.M. Kauzlarich, V. Taufour, Robust antiferromagnetism in $Y_2Co_3$, Phys. Rev. B 104 (2021) 184407. https://doi.org/10.1103/PhysRevB.104.184407

[85] F.T. Parker, H. Oesterreicher, Magnetic-Properties of $La_2Ni_7$, J Less-Common Met 90 (1983) 127-136. https://doi.org/10.1016/0022-5088(83)90124-8
[86] S.V. Meschel, O.J. Kleppa, Thermochemistry of alloys of transition metals and lanthanide metals with some IIIB and IVB elements in the periodic table, J. Alloys Compd. 321 (2001) 183-200. https://doi.org/10.1016/S0925-8388(01)00966-5
[87] A. Provino, S. Steinberg, V. Smetana, U. Paramanik, P. Manfrinetti, S.K. Dhar, A.-V. Mudring, Gold in the layered structures of $R_3Au_7Sn_3$: from relativity to versatility, Cryst. Growth Des. 16 (2016) 5657-5668. https://doi.org/10.1021/acs.cgd.6b00478
[88] C. Celania, V. Smetana, A. Provino, V. Pecharsky, P. Manfrinetti, A.-V. Mudring, $R_3Au_9Pn$ (*R* = Y, Gd–Tm; *Pn* = Sb, Bi): A Link between $Cu_{10}Sn_3$ and $Gd_{14}Ag_{51}$, Inorg. Chem. 56 (2017) 7247-7256. https://doi.org/10.1021/acs.inorgchem.7b00898
[89] M.L. Rhodehouse, T. Bell, V. Smetana, A.-V. Mudring, G.H. Meyer, From the Nonexistent Polar Intermetallic $Pt_3Pr_4$ via $Pt_{2-x}Pr_3$ to Pt/Sn/Pr Ternaries, Inorg. Chem. 57 (2018) 9949-9961. https://doi.org/10.1021/acs.inorgchem.8b01121